Topological Properties of Linear Circuit Lattices

Victor V. Albert,* Leonid I. Glazman,† and Liang Jiang‡
Departments of Applied Physics and Physics, Yale University, New Haven, Connecticut, USA
(Received 23 October 2014; published 30 April 2015)

Motivated by the topologically insulating circuit of capacitors and inductors proposed and tested by Jia *et al.* [arXiv:1309.0878], we present a related circuit with fewer elements per site. The normal mode frequency matrix of our circuit is unitarily equivalent to the hopping matrix of a quantum spin Hall insulator, and we identify perturbations that do not backscatter the circuit's edge modes. The idea behind these models is generalized, providing a platform to simulate tunable and locally accessible lattices with arbitrary complex spin-dependent hopping of any range. A simulation of a non-Abelian Aharonov-Bohm effect using such linear circuit designs is discussed.

DOI: 10.1103/PhysRevLett.114.173902 PACS numbers: 42.70.Qs, 03.65.Vf, 78.67.Pt

The realization that electrons propagating on the edges of two-dimensional (2D) topological insulators at zero temperature are protected from certain disorder [1–5] has spurred research simulating these and similar edge effects in photonic or phononic systems [6–9] (reviewed in Ref. [10]). The existence of edge modes whose energies lie within a given bulk gap of a noninteracting tight-binding Hamiltonian can be traced to a certain property of the corresponding hopping matrix [11]. Namely, a "topologically nontrivial" hopping matrix is characterized by having a nontrivial value of some topological invariant at that bulk gap. Therefore, the problem of engineering edge modes in bosonic systems can be reduced to making sure that the time evolution is governed by some topologically nontrivial matrix. Many efforts emulate the electronic systems that inspired us, but over time we should be able to construct a wider variety of systems than those readily available in nature (e.g., Ref. [12]). While edge mode protection in topologically nontrivial bosonic systems may not be as intrinsic or robust (e.g., protection is not guaranteed by time-reversal symmetry; see Box 2 of Ref. [10]), these directions should nevertheless advance understanding and could offer novel applications of the materials in question.

In this Letter, we discuss topologically insulating (TI) circuits [13]—lattices of inductors and capacitors whose normal mode frequency matrix Ω^2 mimics a topologically nontrivial hopping matrix of an electronic system. Topological photonics includes many proposals [6,7]; here, we study only inductors and capacitors with the goal of providing the simplest building blocks that can lead to topological nontriviality. We discuss a minimal example [Fig. 1(a)] whose Ω^2 matrix is (unitarily) equivalent to the hopping matrix of a spinful 2D electron gas in a magnetic field (see Sec. 5.2 in Ref. [14]), i.e., a spin-doubled Azbel-Hofstadter model [15] (deemed the time-reversal invariant (TRI) Hofstadter model [16]). Our example simulates $1/3$ magnetic flux per plaquette. Such a model is (topologically) similar to the spin-doubled Haldane model lattice [17] (see Sec. 9.1.2 in Ref. [14]) that is featured in the more general Kane-Mele $\mathbb{Z}_2$ topological insulator [1,2]. We determine how features of such models carry over to the circuit context, summarized in Table I. The first TI circuit, which has already been realized [13], is a simple extension of our example, and we outline that design in the Supplemental Material [18]. We further generalize the recipe and provide a method to construct Ω^2 equivalent to the hopping matrix of a lattice of spins with arbitrary

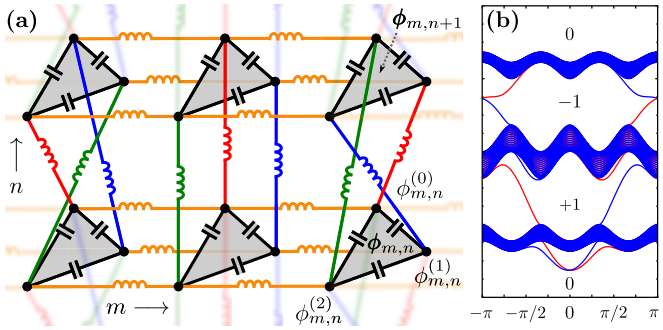

FIG. 1 (color online). (a) Circuit diagram of a TI circuit lattice, whose normal mode frequency matrix Ω^2 is equivalent to the hopping matrix of the spin-doubled Hofstadter model in the Landau gauge with respective $\pm 1/3$ magnetic flux per plaquette. All inductors (capacitors) have uniform inductance (capacitance), so colors are used for visual aid only. The lattice consists of triangular sites m, n (labeled as $\boldsymbol{\phi}_{m,n}$, shaded gray), each consisting of three integrated voltages $\phi^{(\mu)}_{m,n}$ ($\mu = 0, 1, 2$) at its nodes. The vertical inductive connection is dependent on the horizontal index m and generated by the cyclic wiring permutation V_y in Eq. (1). (b) Band structure of Ω^2 simulating a semi-infinite sample, i.e., a wide vertical strip with the left edge consisting of $(V_y)^0$ permutations and right edge mode bands removed. Bands for the spin up (down) component of the TRI Hofstadter model are in red (blue). The spin Chern number $\mathcal{C}_{\mathrm{sc}}$ (see text) is written inside each gap. The edge modes below the lowest bulk band arise because of circuit edge effects [27] and are not topologically protected because they do not traverse a gap.

complex spin-dependent hopping. Notably, we show how to simulate *any* $U(1)$ hopping with a smaller circuit than that of Ref. [13], which simulated a *specific* $U(1)$ hopping. This provides a platform to synthesize background gauge fields using linear circuits in parallel to studies with more complex elements [7,21] and to intense investigations using ultracold atoms (e.g., Refs. [22–25] and refs. therein).

Minimal example.—We distill the idea from Ref. [13] in the form of a simplified example [Fig. 1(a)] and detail how our methods and conclusions apply to Ref. [13] elsewhere (Supplemental Material [18]). Our circuit consists of a lattice of sites (gray), with each site consisting of three nodes. Inductors link sites to each other while capacitors couple the nodes within a site. We stress that no external flux is threaded through any loop of the circuit, and the magnetic flux of the Hofstadter model is *simulated* via the intersite inductive wiring. Transforming the real normal mode frequency matrix Ω^2 into the form of a Hofstadter hopping matrix consists of grouping degrees of freedom into vectors and performing a transformation to complex variables. In an ungrounded circuit, each node m, n, μ (with $\mu = 0, 1, 2$ labeling the degrees of freedom of the site) has a time-integrated absolute voltage $\phi^{(\mu)}_{m,n} \equiv \int_{-\infty}^{t} v^{(\mu)}_{m,n}(t')dt'$ associated with it [26]. This labeling scheme introduces redundant degrees of freedom (which will soon be removed), but allows Ω^2 to be determined analytically. We now group the nodes at each site m, n into a vector $\boldsymbol{\phi}^{\mathsf{T}}_{m,n} = \langle \phi^{(0)}_{m,n}, \phi^{(1)}_{m,n}, \phi^{(2)}_{m,n} \rangle$. For example, the Lagrangian contribution of the link between site m, n and m, $n+1$ [see Fig. 1(a)] is then organized into a (kinetic) capacitive part $\frac{1}{2}\sum_{\delta=0,1} \dot{\boldsymbol{\phi}}^{\mathsf{T}}_{m,n+\delta} C_0 \dot{\boldsymbol{\phi}}_{m,n+\delta}$ and a (potential) inductive part

$$\frac{1}{2}\left(\sum_{\delta=0,1} \boldsymbol{\phi}^{\mathsf{T}}_{m,n+\delta} I_3 \boldsymbol{\phi}_{m,n+\delta} - \boldsymbol{\phi}^{\mathsf{T}}_{m,n} V_y \boldsymbol{\phi}_{m,n+1} - \boldsymbol{\phi}^{\mathsf{T}}_{m,n+1} V_y^{\mathsf{T}} \boldsymbol{\phi}_{m,n} \right)$$

with I_n $n \times n$ identity and respective onsite and intersite couplings

$$C_0 = \frac{1}{3}\begin{pmatrix} 2 & -1 & -1 \\ -1 & 2 & -1 \\ -1 & -1 & 2 \end{pmatrix} \quad \text{and} \quad V_y = \begin{pmatrix} 0 & 1 & 0 \\ 0 & 0 & 1 \\ 1 & 0 & 0 \end{pmatrix}. \tag{1}$$

Above, $(V_y)_{01}$, $(V_y)_{12}$, and $(V_y)_{21}$ correspond respectively to the red, blue, and green circuit elements from Fig. 1(a), and we have set a uniform capacitance of $1/3$ (for normalization) and inductance of 1. The equation of motion (EOM) for $\boldsymbol{\phi}_{m,n}$ in the lattice from Fig. 1(a) is

$$\begin{aligned} C_0 \ddot{\boldsymbol{\phi}}_{m,n} = &-4\boldsymbol{\phi}_{m,n} + V_x \boldsymbol{\phi}_{m+1,n} + V_x^{\mathsf{T}} \boldsymbol{\phi}_{m-1,n} \\ &+ (V_y)^m \boldsymbol{\phi}_{m,n+1} + (V_y^{\mathsf{T}})^m \boldsymbol{\phi}_{m,n-1}, \end{aligned} \tag{2}$$

where $V_x = I_3$ and 4 is the number of nearest neighbors for a site in the bulk. The three distinct powers of V_y [$(V_y)^3 = I_3$] correspond to three vertical inductive wiring permutations and mimic the Hofstadter model in the Landau gauge.

To diagonalize Ω^2 in the index μ and simultaneously remove the aforementioned redundant degrees of freedom, one can apply a discrete Fourier transform F to the three nodes of each site: $\boldsymbol{\zeta}_{m,n} = F\boldsymbol{\phi}_{m,n}$ or $\zeta^{(\mu)}_{m,n} = (1/\sqrt{3}) e^{i(2\pi/3)\mu\nu} \phi^{(\nu)}_{m,n}$ ($\mu, \nu \in \{0, 1, 2\}$ and repeated indices summed). This site-preserving transformation to a complex vector $\boldsymbol{\zeta}^{\mathsf{T}}_{m,n} = \langle \zeta^{(0)}_{m,n}, \zeta^{(1)}_{m,n}, \zeta^{(2)}_{m,n} \rangle$ block diagonalizes Ω^2 in μ at the expense of introducing complex numbers. In the $\boldsymbol{\zeta}$ basis, the simultaneously diagonal capacitive and inductive coupling matrices are $\tilde{C}_0 = \mathrm{diag}(0,1,1)$, $\tilde{V}_y = \mathrm{diag}(1, e^{i(2\pi/3)}, e^{-i(2\pi/3)})$, and $\tilde{V}_x = V_x = I_3$. Since the transformed circuit Lagrangian does not contain $\dot{\zeta}^{(0)}_{m,n}$ terms [since $(\tilde{C}_0)_{00} = 0$], the $\zeta^{(0)}_{m,n} \equiv \sum_\mu \phi^{(\mu)}_{m,n}$ component for each site represents "half" of a degree of freedom (akin to a classical harmonic oscillator in the limit of zero mass) and can be thought of as an ordinary normal mode in the limit of zero capacitance. The EOM for $\left\{ \zeta^{(1)}_{m,n}, \zeta^{(1)\star}_{m,n} = \zeta^{(2)}_{m,n} \right\}$, treated as independent full degrees of freedom ($j = 1, 2$), is

$$\begin{aligned} \ddot{\zeta}^{(j)}_{m,n} = &-4\zeta^{(j)}_{m,n} + \zeta^{(j)}_{m+1,n} + \zeta^{(j)}_{m-1,n} \\ &+ e^{i(2\pi/3)mj} \zeta^{(j)}_{m,n+1} + e^{-i(2\pi/3)mj} \zeta^{(j)}_{m,n-1}. \end{aligned} \tag{3}$$

These variables are linear superpositions of bosonic modes, and their hopping properties resemble the TRI Hofstadter model in the Landau gauge; i.e., they acquire a (simulated) Peierls phase upon a vertical hopping. Thus, the block-diagonal normal mode frequency matrix $\tilde{\Omega}^2 = \bigoplus_\mu \tilde{\Omega}^2_\mu$ consists of the trivial mode matrix $\tilde{\Omega}^2_0$ and the matrices $\tilde{\Omega}^2_{1,2}$ forming the spin-doubled Hofstadter model.

Topological invariant.—In Fig. 1(b), the band structure of $\tilde{\Omega}^2_1$ ($\tilde{\Omega}^2_2$) is plotted in red (blue), depicting slightly distorted [27] counterpropagating edge modes. Since the pseudospin $\langle \zeta^{(1)}, \zeta^{(2)} \rangle$ is conserved, the spin-doubled Hofstadter model is characterized by the $\mathbb{Z}$ spin Chern number $\mathcal{C}_{\mathrm{sc}} = \frac{1}{2}(\mathcal{C}_1 - \mathcal{C}_2)$ [4] at each gap. Given an edge, the Chern numbers $\mathcal{C}_j$ are related to the number of times the edge modes of $\tilde{\Omega}^2_j$ wind around a horizontal line drawn in the gap (Secs. 5.3.1 and 6.4 in Ref. [14]). Moreover, the quantity $\mathcal{C} = \mathcal{C}_{\mathrm{sc}} \mathrm{mod} 2$ determines whether there is an even or odd number of pairs of counterpropagating edge modes (this is the invariant of the more general $\mathbb{Z}_2$ TI [2], a quantum spin Hall insulator, QSHI, with no spin conservation). The invariant $\mathcal{C}$ is characterized by Kramers degeneracy, which prohibits elastic backscattering between counterpropagating edge modes only for odd numbers of edge mode pairs per edge [28]. Both our example and Ref. [13] contain one gapless edge mode pair per edge ($\mathcal{C}_{\mathrm{sc}} = 1$) and, since pseudospin is conserved, constitute a

QSHI. Moreover, this system is not a crystalline topological insulator [29] (as defined in Ref. [30]) since $\mathcal{C} \neq 0$.

Because of the invariants established above, there must exist some operator in the circuit context that mimics the antiunitary electronic time-reversal operator $i\sigma_2 K$ (with $Ki = -iK$ and $\sigma_{1,2,3}$ the usual Pauli matrices), squares to $-I_2$, and generates a Kramers degeneracy (a similar observation has been made [9] with photonic TIs [8]). Such an operator does indeed exist and comes about from a symmetry of the circuit. In the $\boldsymbol{\phi}$ basis, the coupling matrix V_y, a cyclic permutation of all nodes in each site, commutes with Ω^2 and generates the symmetry group $C_3 \approx \{I_3, V_y, V_y^\mathsf{T}\}$. A generic linear commuting operator (with identity components in the dimensions indexed by m, n) can be expressed as $c_\mu (V_y)^\mu$ for some $c_{\mu=0,1,2} \in \mathbb{C}$. Since V_y is real, all antilinear extensions of the above operators can be expressed as $c_\mu (V_y)^\mu K$. In the $\boldsymbol{\zeta}$ basis,

$$K \to \tilde{K} = F^\dagger K F = F^\dagger F^\star K = (1 \oplus \sigma_1) K,$$

which squares to I_3. However, the operator S [such that $\tilde{S} = (1 \oplus \sigma_2)K$ and $\tilde{S}^2 = 1 \oplus (-I_2)$] is also in the span of $(V_y)^\mu K$. Thus, electronic time-reversal symmetry in the tight-binding context maps to a combination of ordinary time-reversal and cyclic permutations in the circuit context. We also note that $\tilde{\Sigma} = \tilde{S}\tilde{K} = 1 \oplus (-i\sigma_3)$ characterizes the conserved pseudospin for the time-reversed Hofstadter copies.

Symmetry protection.—Mirroring topological protection in QSHIs and $\mathbb{Z}_2$ TIs, counterpropagating edge modes of a TI circuit must also be "protected" to some degree. Emulating one-particle elastic scattering processes in TRI electronic systems [28], a crossing between edge modes on the same edge at time-reversal invariant points $k = 0, \pi$ in the Brillouin zone will not be lifted by inductance or capacitance perturbations that commute with S (which is now in the $\boldsymbol{\phi}$ basis). Let a generic inductive link between sites m, n and p, q be parametrized by

$$\begin{aligned} &\boldsymbol{\phi}_{m,n}^\mathsf{T} M_{11} \boldsymbol{\phi}_{m,n} + \boldsymbol{\phi}_{p,q}^\mathsf{T} M_{22} \boldsymbol{\phi}_{p,q} \\ &\quad + \boldsymbol{\phi}_{m,n}^\mathsf{T} M_{12} \boldsymbol{\phi}_{p,q} + \boldsymbol{\phi}_{p,q}^\mathsf{T} M_{12}^\mathsf{T} \boldsymbol{\phi}_{m,n}, \end{aligned} \tag{4}$$

where real 3×3 matrices M_{jj} $(j = 1, 2)$ are on-site couplings at the two respective sites and M_{12} is the intersite coupling. Such a perturbation will not cause elastic backscattering between edge modes whenever $[M_{jj'}, S] = 0$. For our design, such perturbations are all those which do not break the circuit's C_3 symmetry, i.e., commute with V_y. For example, an identical simultaneous perturbation of all three inductances in any given link [$M_{jj} \propto I_3$, $M_{12} \propto (V_y)^\mu$] or an on-site perturbation $(M_{jj'} \propto \delta_{j1}\delta_{j'1}[(V_y)^\mu + (V_y^\mathsf{T})^\mu])$ will not mix edge modes. However, fluctuations of inductance *will* cause elastic backscattering between edge modes whenever the fluctuations are *not* identical within any given link. A similar statement holds for capacitive perturbations.

Topologically insulating circuits (i.e., both our design and Ref. [13]) turn out to be similar to certain optical resonator designs [7] in that both are robust against disorder that does not induce flips of pseudospin [10]. In our design, the pseudospin is characterized by $\Sigma = SK$: since $M_{jj'}$ are real matrices, $[M_{jj'}, S] = 0 \leftrightarrow [M_{jj'}, \Sigma] = 0$. We also note that, in a realistic setup, both optical resonator edge states and TI circuit edge modes will decay due to optical and microwave dissipation, respectively.

Generalizations.—Given that the above design only has $d = 3$ nodes per site, one can consider increasing the number of nodes per site (triangles $\to$ d-gons) and generalizing the cyclic permutation ($V_y \to \sum_{\mu=0}^{d-1} |\mu\rangle\langle\mu + 1|\mathrm{mod}d$). This results in a family of models that can emulate TRI Hofstadter hopping matrices with p/d background magnetic flux using d nodes per site and vertical connections $(V_y)^p$ (with integer p). We note in passing that the $d = 2$ case is trivial because it is not gapped in the bulk [see Eq. (5.53) in Ref. [14]] and that Ref. [13] is closely related to $d = 4$ (Supplemental Material [18]). However, we have developed other generalizations that allow the simulation of any background gauge field using circuits that are much more compact. We discuss these approaches below.

First, an *arbitrary* complex hopping can be achieved using only three nodes per site. For simplicity, we first focus on one link. Instead of having one wiring permutation (e.g., V_y in Fig. 1), one can implement all three permutations $(V_y)^\mu$ in a linear superposition [Fig. 2(a)]. In this case, each permutation gains its own degree of freedom. The intersite

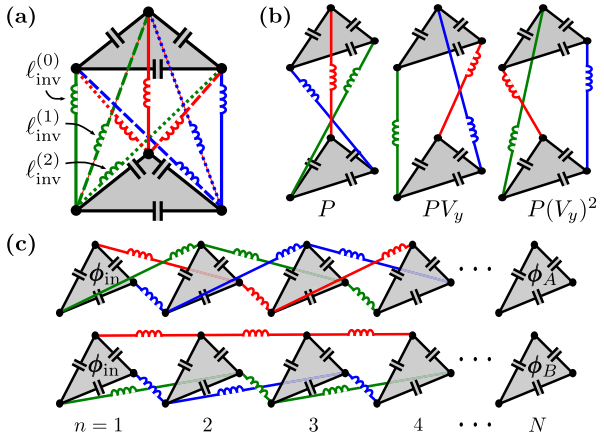

FIG. 2 (color online). (a) Superposition of three different wiring permutations $(V_y)^\mu$ and their respective inverse inductances $\ell_{\mathrm{inv}}^{(\mu)}$, $\mu = 0, 1, 2$ (solid, dashed, dotted lines, respectively), achieving any $U(1)$ hopping in the $\boldsymbol{\zeta}$ basis. (b) Additional wiring permutations $P(V_y)^\mu$ which create $U(2)$ hopping terms in the $\boldsymbol{\zeta}$ basis. (c) A circuit to simulate the Aharonov-Bohm effect. A vector signal $\boldsymbol{\phi}_{\mathrm{in}}$ enters from the left, propagates through N sites via two different paths A and B, and produces two outputs, $\boldsymbol{\phi}_{A,B}$. One can measure an interference between these outputs [Eq. (7)] and observe oscillations for even N since permutations V_y and P do not commute.

inductive coupling matrix is then $V_y \to V_A = \ell_{\rm inv}^{(\mu)}(V_y)^\mu$, where $\ell_{\rm inv}^{(\mu)}$ is the inverse inductance of permutation μ. In the $\boldsymbol{\zeta}$ basis, the coupling is diagonal with $(\tilde{V}_A)_{\mu\nu} = \ell_{\rm inv}^{(\tau)} e^{i(2\pi/3)\tau\nu}\delta_{\mu\nu}$ (no sum over ν). Parametrizing the $\mu = 1$ component in terms of an amplitude and phase yields $(\tilde{V}_A)_{11} = t_A e^{i\theta_A}$ with

$$t_A = \sqrt{\left[\ell_{\rm inv}^{(0)} - \frac{1}{2}(\ell_{\rm inv}^{(1)} + \ell_{\rm inv}^{(2)})\right]^2 + \frac{3}{4}(\ell_{\rm inv}^{(1)} - \ell_{\rm inv}^{(2)})^2},$$

$$\theta_A = \tan^{-1}\left(\frac{\sqrt{3}(\ell_{\rm inv}^{(1)} - \ell_{\rm inv}^{(2)})}{2\ell_{\rm inv}^{(0)} - (\ell_{\rm inv}^{(1)} + \ell_{\rm inv}^{(2)})}\right). \quad (5)$$

Naturally, $(\tilde{V}_A)_{00} = \sum_\mu \ell_{\rm inv}^{(\mu)} \equiv \lambda_A$ and $(\tilde{V}_A)_{22} = t_A e^{-i\theta_A}$. Additionally, there is a diagonal inductance contribution of $\frac{1}{2}\lambda_A \boldsymbol{\zeta}^\dagger\boldsymbol{\zeta}$ to both of the linked sites. Thus, the hopping and diagonal terms $\{t_A, \theta_A, \lambda_A\}$ can be tuned using $\{\ell_{\rm inv}^{(\mu)}\}_{\mu=0}^2$ with the constraint $\lambda_A \geq t_A$ since $\ell_{\rm inv}^{(\mu)} \geq 0$. The symmetry protection still holds here since $(V_y)^\mu \in C_3$.

Second, non-Abelian couplings can straightforwardly be implemented while still keeping $d = 3$. Instead of using the permutations $(V_y)^\mu$, three other permutations $P(V_y)^\mu$ [with $P = 1 \oplus \sigma_1$ and $[P, V_y] \neq 0$; see Fig. 2(b)] can be superimposed to give an inverse inductance coupling matrix $V_y \to V_{NA} = \ell_{\rm inv}^{(\mu)} P(V_y)^\mu$. Nonzero entries of $\tilde{V}_{NA}$ are an off-diagonal hopping $(\tilde{V}_{NA})_{12} = (\tilde{V}_{NA})_{21}^\star \equiv t_{NA} e^{i\theta_{NA}}$ and a diagonal contribution $(\tilde{V}_{NA})_{00} = \sum_\mu \ell_{\rm inv}^{(\mu)} \equiv \lambda_{NA}$. Similar to V_A, the hopping and diagonal terms $\{t_{NA}, \theta_{NA}, \lambda_{NA}\}$ of V_{NA} can be tuned using $\{\ell_{\rm inv}^{(\mu)}\}_{\mu=0}^2$. As an example, one can already realize a non-Abelian generalization of the Hofstadter model [23] by letting $V_x \to P$ in Eq. (2).

The above design allows one to create a lattice with spatially nonuniform noncommuting unitary hoppings between sites [e.g., $t_{m,n}\exp(i\theta_{m,n})$ using either $(V_y)^\mu$ or $P(V_y)^\mu$] while maintaining identical on-site contributions ($\lambda_{m,n} \equiv \lambda$). Despite this flexibility, one cannot create arbitrary $U(2)$ hoppings using three nodes per site (assuming on-site contributions are to remain identical). This is because linear superpositions of the six permutations [$(\tilde{V}_y)^\mu$ and $P(\tilde{V}_y)^\mu$] with *nonnegative real coefficients* (since our variables are inverse inductances) do not span all unitary 2×2 matrices acting on $\langle \zeta^{(1)}, \zeta^{(2)} \rangle$. More permutations are needed, so one needs more nodes per site to generate them. Finding this minimal number of nodes maps to an open problem from group theory [31,32], and we have determined that one needs at most n^2 nodes per site to simulate unitary hoppings of dimension $n > 2$ (Supplemental Material [18]).

Non-Abelian Aharonov-Bohm effect.—We finish with a discussion of applications. First, we propose an experiment that uses the $\boldsymbol{\phi}$-$\boldsymbol{\zeta}$ duality to observe an electrical non-Abelian Aharonov-Bohm (AB) effect [23,24,33]. Since all circuit elements are reciprocal here, it is the nonreciprocity of their permutations that leads to interference effects. One can think of $\boldsymbol{\phi}$ as the wave functions and sites $n = 1, 2, \ldots, N$ as spatial positions [Fig. 2(c)]. An incoming signal $\boldsymbol{\phi}_{\rm in}^{\mathsf{T}} = \langle \phi_{\rm in}^{(0)}, \phi_{\rm in}^{(1)}, \phi_{\rm in}^{(2)} \rangle$ is applied onto paths A and B. Let

$$\phi_{\rm in}^{(\mu)} = \sqrt{\frac{2}{3}}\cos\left(\omega t - \frac{2\pi}{3}\mu\right), \quad (6)$$

which is equivalent to $\boldsymbol{\zeta}_{\rm in}^{\mathsf{T}} = (1/\sqrt{2})\langle 0, e^{i\omega t}, e^{-i\omega t}\rangle$. Path A contains $N-1$ cyclic permutations V_y from Eq. (1) while path B consists of $N-1$ permutations P from Fig. 2(b) (with $[V_y, P] \neq 0$). Remembering Eq. (3), we see that a phase of $e^{i(2\pi/3)}$ ($e^{-i(2\pi/3)}$) is gained by $\zeta^{(1)}$ ($\zeta^{(2)}$) as the signal "hops" sites in path A. For path B, the $\zeta^{(1)}$ and $\zeta^{(2)}$ components are exchanged upon each application of P. One can superimpose the outputs $\boldsymbol{\phi}_A$ and $\boldsymbol{\phi}_B$ to observe their interference. For odd N, this interference is constant in time. For even N, one should see oscillations due to a nontrivial path B,

$$|\boldsymbol{\phi}_A + \boldsymbol{\phi}_B|^2 \propto \cos^2\left\{\omega t - \frac{2\pi}{3}[(N-1)\bmod 3]\right\}. \quad (7)$$

Since voltage is the derivative of ϕ, one can perform the above experiment by applying voltage signals of the form of $\boldsymbol{\phi}_{\rm in}$ from Eq. (6), measuring the six output signals at site N for paths A and B, and superimposing them in the manner of Eq. (7). Since the AB effect is nonreciprocal, driving from right to left ($\boldsymbol{\phi}_{\rm in} \leftrightarrow \boldsymbol{\phi}_{A,B}$) should flip the sign of the phase gained along A.

Outlook.—This work generalizes the first realization of a TI circuit [13]. We present a simplified circuit whose normal mode frequency matrix is unitarily equivalent to the hopping matrix of the time-reversal invariant Hofstadter model [16] with $1/3$ magnetic flux per plaquette. A summary of the equivalence is in Table I. Since Hofstadter models posses edge modes, we determine which perturbations do not cause edge modes to backscatter.

Additionally, we generalize the approach and determine the minimal circuit complexity required to simulate non-Abelian background gauge fields. Besides a simulation of

TABLE I. Summary of the equivalence between the Hofstadter model and a TI circuit. $\phi_{m,n}^{(\mu)}$ is the integrated voltage at node m, n, μ, as depicted in Fig. 1(a), σ_2 is the second Pauli matrix, and $Ki = -iK$.

TRI Hofstadter model	TI circuit
Hopping matrix	Normal mode frequency matrix Ω^2
Spinful fermion $c_{m,n} = \left(c_{m,n}^{(1)}, c_{m,n}^{(2)}\right)$	$\left(\zeta_{m,n}^{(1)}, \zeta_{m,n}^{(1)*}\right)$ with $\zeta_{m,n}^{(1)} = e^{i(2\pi/3)\nu}\phi_{m,n}^{(\nu)}$
Peierls phase	Intersite wiring permutations
Kramers degeneracy	$\tilde{S} = (1 \oplus \sigma_2)K$ due to C_3 symmetry

the Aharonov-Bohm effect, we now speculate on further applications of this circuit QED simulation tool [34]. A major flexibility is being able to construct and locally probe virtually any lattices (e.g., honeycomb [25] or kagome [35]) and lattices with connections other than nearest neighbor at the same cost in complexity. Almost any physically relevant and exotic geometry can be implemented [36] (e.g., a Möbius strip [13]). One can construct interfaces of lattices and observe mixing of edge modes at the boundary, akin to graphene p-n junctions [37]. To simulate interactions, one can substitute Josephson junctions [38] (mechanical oscillators [39]) for inductors (capacitors). These and other topics are currently under investigation.

We thank J. Simon, D. Schuster, A. Dua, T. Morimoto, B. Elias, W. C. Smith, S. M. Girvin, M. H. Devoret, B. Bradlyn, Z. Minev, and A. Petrescu for fruitful discussions. We thank one of the referees for pointing out the possibility of simulating a magnetic flux of p/d with $p \neq 1$. This work was supported, in part, by the National Science Foundation (NSF) Graduate Research Fellowship Program under Grant DGE-1122492 (V. V. A.); NSF Grant DMR-1206612 (L. I. G.); and the Army Research Office, Air Force Office of Scientific Research Multidisciplinary Research Program of the University Research Initiative, Defense Advanced Research Projects Agency Quiness program, the Alfred P. Sloan Foundation, and the David and Lucile Packard Foundation (L. J.).

Note added.—After completion of this work, we learned that an acoustic analogue of the 1/3 TRI Hofstadter model has been implemented in Ref. [40].

*valbert4@gmail.com
†leonid.glazman@yale.edu
‡liang.jiang@yale.edu

[1] C. L. Kane and E. J. Mele, Phys. Rev. Lett. **95**, 226801 (2005).
[2] C. L. Kane and E. J. Mele, Phys. Rev. Lett. **95**, 146802 (2005).
[3] L. Sheng, D. N. Sheng, C. S. Ting, and F. D. M. Haldane, Phys. Rev. Lett. **95**, 136602 (2005).
[4] D. N. Sheng, Z. Y. Weng, L. Sheng, and F. D. M. Haldane, Phys. Rev. Lett. **97**, 036808 (2006).
[5] B. A. Bernevig and S.-C. Zhang, Phys. Rev. Lett. **96**, 106802 (2006).
[6] S. Raghu and F. D. M. Haldane, Phys. Rev. A **78**, 033834 (2008); Z. Wang, Y. D. Chong, J. D. Joannopoulos, and M. Soljačić, Nature (London) **461**, 772 (2009); J. Koch, A. A. Houck, K. Le Hur, and S. M. Girvin, Phys. Rev. A **82**, 043811 (2010); R. O. Umucalilar and I. Carusotto, Phys. Rev. A **84**, 043804 (2011); Y. E. Kraus, Y. Lahini, Z. Ringel, M. Verbin, and O. Zilberberg, Phys. Rev. Lett. **109**, 106402 (2012); K. Fang, Z. Yu, and S. Fan, Nat. Photonics **6**, 782 (2012); T. Ochiai, Phys. Rev. B **86**, 075152 (2012); G. Q. Liang and Y. D. Chong, Phys. Rev. Lett. **110**, 203904 (2013); M. C. Rechtsman, J. M. Zeuner, A. Tünnermann, S. Nolte, M. Segev, and A. Szameit, Nat. Photonics **7**, 153 (2012); M. C. Rechtsman, J. M. Zeuner, Y. Plotnik, Y. Lumer, D. Podolsky, F. Dreisow, S. Nolte, M. Segev, and A. Szameit, Nature (London) **496**, 196 (2013); M. Verbin, O. Zilberberg, Y. E. Kraus, Y. Lahini, and Y. Silberberg, Phys. Rev. Lett. **110**, 076403 (2013); L. Lu, L. Fu, J. D. Joannopoulos, and M. Soljačić, Nat. Photonics **7**, 294 (2013); A. R. Davoyan and N. Engheta, Phys. Rev. Lett. **111**, 257401 (2013); V. Peano, C. Brendel, M. Schmidt, and F. Marquardt, arXiv:1409.5375; A. V. Nalitov, D. D. Solnyshkov, and G. Malpuech, arXiv:1409.6564 [Phys. Rev. Lett. (to be published)]; Y.-T. Wang, P.-G. Luan, and S. Zhang, arXiv:1411.2806; T. Karzig, C.-E. Bardyn, N. Lindner, and G. Refael, arXiv:1406.4156; C.-E. Bardyn, T. Karzig, G. Refael, and T. C. H. Liew, arXiv:1409.8282.
[7] M. Hafezi, E. A. Demler, M. D. Lukin, and J. M. Taylor, Nat. Phys. **7**, 907 (2011); S. Mittal, J. Fan, S. Faez, A. Migdall, J. M. Taylor, and M. Hafezi, Phys. Rev. Lett. **113**, 087403 (2014);
[8] A. B. Khanikaev, S. H. Mousavi, W.-K. Tse, M. Kargarian, A. H. MacDonald, and G. Shvets, Nat. Mater. **12**, 233 (2013).
[9] C. He, X.-C. Sun, X.-P. Liu, Z.-W. Liu, Y. Chen, M.-H. Lu, and Y.-F. Chen, arXiv:1401.5603.
[10] L. Lu, J. D. Joannopoulos, and M. Soljačić, Nat. Photonics **8**, 821 (2014).
[11] A. Yu. Kitaev, AIP Conf. Proc. **1134**, 22 (2009).
[12] T. D. Stanescu, V. Galitski, and S. Das Sarma, Phys. Rev. A **82**, 013608 (2010).
[13] N. Jia, A. Sommer, D. Schuster, and J. Simon, arXiv:1309.0878.
[14] B. A. Bernevig and T. L. Hughes, *Topological Insulators and Topological Superconductors* (Princeton University Press, Princeton and Oxford, 2013).
[15] M. Y. Azbel, J. Exp. Theor. Phys. **19**, 634 (1964); D. Hofstadter, Phys. Rev. B **14**, 2239 (1976).
[16] D. Cocks, P. P. Orth, S. Rachel, M. Buchhold, K. Le Hur, and W. Hofstetter, Phys. Rev. Lett. **109**, 205303 (2012); P. P. Orth, D. Cocks, S. Rachel, K. L. Hur, and W. Hofstetter, J. Phys. B **46**, 134004 (2013); L. Wang, H.-H. Hung, and M. Troyer, Phys. Rev. B **90**, 205111 (2014).
[17] F. D. M. Haldane, Phys. Rev. Lett. **61**, 2015 (1988).
[18] See the Supplemental Material at http://link.aps.org/supplemental/10.1103/PhysRevLett.114.173902, which cites Refs. [19,20], for a comparison of this work to Ref. [13] as well as details on the non-Abelian generalization.
[19] M. R. Kibler, J. Phys. A **42**, 353001 (2009).
[20] W. Bosma, J. Cannon, and C. Playoust, J. Symb. Comput. **24**, 235 (1997).
[21] E. Kapit, Phys. Rev. A **87**, 062336 (2013); M. Hafezi, P. Adhikari, and J. M. Taylor, Phys. Rev. B **90**, 060503(R) (2014).
[22] F. Gerbier, N. Goldman, M. Lewenstein, and K. Sengstock, J. Phys. B **46**, 130201 (2013); M. Aidelsburger, M. Lohse, C. Schweizer, M. Atala, J. T. Barreiro, S. Nascimbène, N. R. Cooper, I. Bloch, and N. Goldman, Nat. Phys. **11**, 162 (2015).
[23] K. Osterloh, M. Baig, L. Santos, P. Zoller, and M. Lewenstein, Phys. Rev. Lett. **95**, 010403 (2005).

[24] A. Jacob, P. Ohberg, G. Juzeliunas, and L. Santos, Appl. Phys. B **89**, 439 (2007).
[25] A. Bermudez, N. Goldman, A. Kubasiak, M. Lewenstein, and M. A. Martin-Delgado, New J. Phys. **12**, 033041 (2010).
[26] M. H. Devoret, in *Quantum Fluctuations*, edited by S. Reynaud, E. Giacobino, and J. Zinn-Justin (Elsevier, New York, 1995), Chap. 10.
[27] Circuit edge effects distort the original TRI Hofstadter spectrum: the 4 from Eq. (3) is replaced by a 3 (2) for sites on edges (corners). Edge modes exist for all three different types of edges of a vertical strip.
[28] X.-L. Qi and S.-C. Zhang, Rev. Mod. Phys. **83**, 1057 (2011).
[29] L. Fu, Phys. Rev. Lett. **106**, 106802 (2011).
[30] B. de Leeuw, C. Küppersbusch, V. Juricic, and L. Fritz, arXiv:1411.0255.
[31] N. Saunders, Austral. Math. Soc. Gaz. **35**, 332 (2008).
[32] B. Elias, L. Silberman, and R. Takloo-Bighash, Exp. Math. **19**, 121 (2010).
[33] K. Fang, Z. Yu, and S. Fan, Phys. Rev. B **87**, 060301 (2013).
[34] A. Aspuru-Guzik and P. Walther, Nat. Phys. **8**, 285 (2012); A. A. Houck, H. E. Tureci, and J. Koch, Nat. Phys. **8**, 292 (2012); S. Ashhab, New J. Phys. **16**, 113006 (2014).
[35] A. Petrescu, A. A. Houck, and K. Le Hur, Phys. Rev. A **86**, 053804 (2012).
[36] D. I. Tsomokos, S. Ashhab, and F. Nori, Phys. Rev. A **82**, 052311 (2010).
[37] D. A. Abanin and L. S. Levitov, Science **317**, 641 (2007).
[38] S. M. Girvin, *Quantum Machines: Measurement and Control of Engineered Quantum Systems*, edited by M. H. Devoret, B. Huard, R. J. Schoelkopf, and L. F. Cugliandolo (Oxford University Press, Oxford, 2014) Chap. 3.
[39] T. A. Palomaki, J. W. Harlow, J. D. Teufel, R. W. Simmonds, and K. W. Lehnert, Nature (London) **495**, 210 (2013); V. B. Braginsky and F. Y. Khalili, *Quantum Measurement*, edited by K. S. Thorne (Cambridge University Press, Cambridge, England, 1992).
[40] R. Süsstrunk and S. D. Huber, arXiv:1503.06808.